A TITANic Catalog of Features & Surface Types Revealed by Cassini SAR and Its Application to Studying Saturn's Largest Moon

Christopher Tsai (tsaic@stanford.edu)

Lauren Catherine Wye (lcwye@stanford.edu)

Professor Howard Zebker (zebker@stanford.edu)

June 28, 2006 – September 1, 2006

Introduction to Titan and Cassini Radar

Titan, Saturn's largest moon with a radius of 2575 km, is difficult to visualize by normal infrared and spectroscopic methods because of its thick, absorbing atmosphere. Thus, the Cassini-Huygens mission uses the microwave RADAR instrument (2.17-cm wavelength) to minimize atmospheric effects. The Huygens probe entered Titan's atmosphere and landed on the surface in January 2005. The Cassini orbiter, halfway through its four-year mission, supplies us with two key measurements: 1) coarse-resolution scatterometer data across a wide range of incidence angles, which will attain near-global coverage, and 2) **high-resolution Synthetic Aperture Radar (SAR) images** acquired at a fixed incidence angle, to cover about 30% of Titan's surface (Elachi et al., 2005b). Cassini has thus far returned SAR images of the regions outlined below, labeled by orbit number, with TA occurring first. We view and study the swaths with our program disfloat to see images like Figure B. These radar reflectivity (normalized radar cross-section, or σ_0) images, as well as their latitude and longitude, are stored in Basic Image Data Record (BIDR) files. The radar reflectivity imaged in Figure B varies with surface slope, roughness, and composition. Brighter regions signify higher reflectivity σ_0.

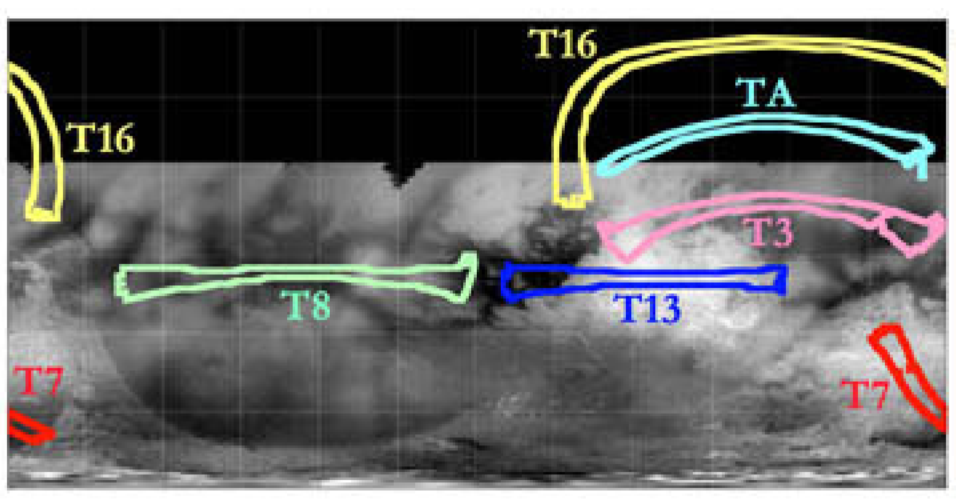

Figure A (Left): High-resolution SAR coverage of Titan, currently spanning ≈10% of surface. By 2008, SAR data will cover ≈30% of the surface.

NOTE: The infrared imaging device used to generate the background cannot view the north polar region, so the area remains uncharted (black).

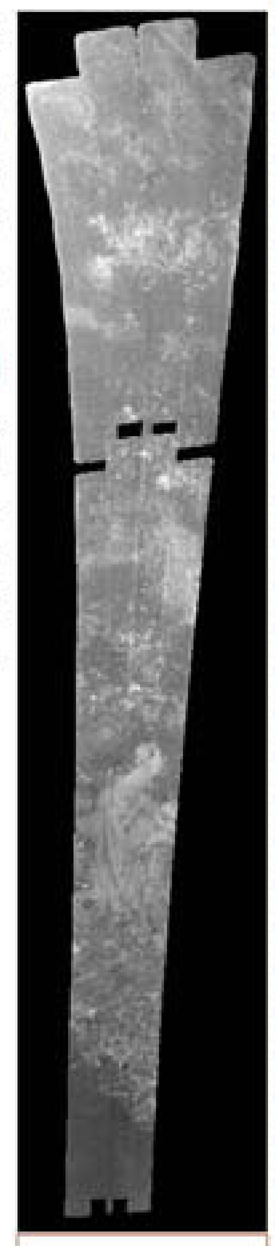

Figure B: T7 σ_0 swath viewed in disfloat

Objective: Compiling a Catalog of Features & Surfaces

The Cassini Team has analyzed data from both the SAR and scatterometer modes, each with its own advantage. The SAR's high-resolution images have allowed scientists to identify specific types of features, such as **dunes, craters, lakes,** and **flows**, and their location on the surface; meanwhile, scatterometer data, with its wide range of incidence angles, reveals the Reflectivity-vs.-Angle relationship, which can be fit with backscatter curves to calculate surface properties.

My research has focused on **classifying features** and **radar reflectivity** seen in SAR images. While the Cassini Radar Team has already identified features, I have been devising ways to **categorize** them systematically in a database of text files. By grouping features of similar types and listing their latitude, longitude, and **average normalized radar cross-section** in text files, the catalog can distinguish precise locations of features and surface terrains, providing a systematic way of studying them in unison and modeling their trends in the scatterometer data, where specific locations are not readily apparent.

Methodology and Measurement Procedure

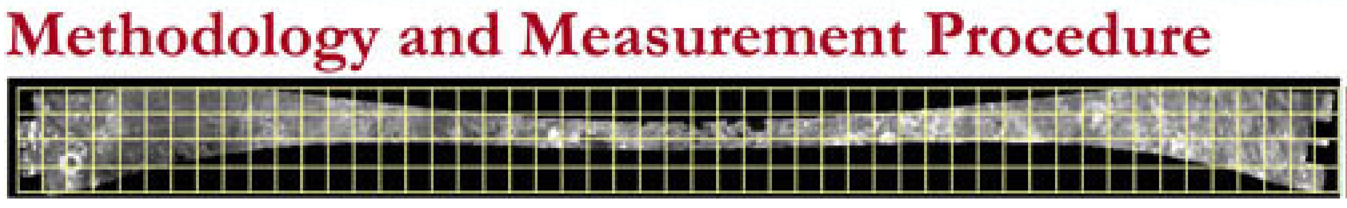

Figure C: Pixels describe σ_0 values, which we box-average in 4x4 sets to compress files.

1. Download and compress noise-subtracted SAR image files to a viewable size.
BIDR files consume hundreds of megabytes; the file is over-magnified, so we compress the image stored in the σ_0 BIDR file by replacing 4x4 sections of pixels with their average value to see more of the surface at once without losing too much feature detail.

2. Discern and catalog detailed features resembling one of several identified types.
Dune fields are most prevalent across imaged regions, but craters, lakes, flows, and vestiges of features also appear. In separate files, we also catalogued unidentified features, such as lines, rings, dots, and peculiar markings. We tagged each feature with its type and the (x,y) coordinates of its bounding polygon's vertices (as shown in Figure D), entering groups into their respective

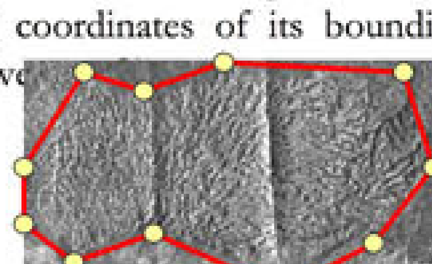

Figure D: The database describes each feature by the vertices of its perimeter.

3. Smoothen the compressed image with an averaging filter.
Low-pass filtering blurs the image and allows us to distinguish large regions with similar normalized radar cross-section or reflectivity (σ_0).

4. Discern and catalog surface regions that share a similar σ_0 value.
Regions sharing a backscatter coefficient could comprise similar material (observing at similar incidence angles removes the angular dependence of σ_0), so we catalog them together.

5. Extract the latitude and longitude of features and regions based on their (x,y) coordinates.
Latitude and longitude values have their own BIDR files, corresponding pixel-for-pixel with the image file. We automate the extraction procedure to produce text file lists and MatLab data vectors for plotting.

7. Systematically compute the average σ_0 value for each region.
A program operating similarly to MatLab's inpolygon averages σ_0 values within a specified boundary.

8. Determine logical bin cutoff values to separate regions of different types in text files.
Each range of values denotes a different surface type, and categorization expedites access to each type.

Normalized Radar Cross-Section (Backscatter Coefficient)

The normalized radar cross-section, also known as the backscatter coefficient, or **reflectivity**, measures the reflective strength of a distributed radar target. It is the radar cross-section per unit area on the surface ground. We can compute values obtained by Cassini Radar by solving the Radar Equation for σ_0:

$$dP_r = \underbrace{P_t G}_{\substack{\text{power transmitted}\\ \text{toward element}}} \; \underbrace{\frac{1}{4\pi R^2}}_{\substack{\text{propagation}\\ \text{to element}}} \; \underbrace{\boxed{\sigma_0}\, dS}_{\substack{\text{backscatter}\\ \text{cross-section}}} \; \underbrace{\frac{1}{4\pi R^2}}_{\substack{\text{propagation back}\\ \text{to receiver}}} \; \underbrace{A_r}_{\substack{\text{effective receiver}\\ \text{aperture}}}$$

dP_r = instantaneous power in one pulse
P_t = power transmitted by radar
G = antenna gain in direction of surface
R = distance from source to surface
dS = differential surface area element

Classification of Titan's Features

Figure E: Lakes of various shapes, sizes, and depths on the T16 swath. Swaths near poles could reveal more.

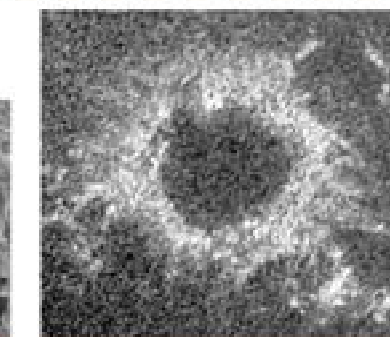

Figure F: Ring/eroded crater (T16)

Figure G: Flows on the left, a cropped impact crater (Menrva) in the center, and a dune patch to the right in T3.

Figure H: The Sinlap Crater (T3)

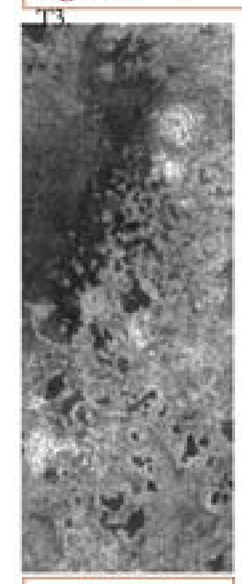

Figure I

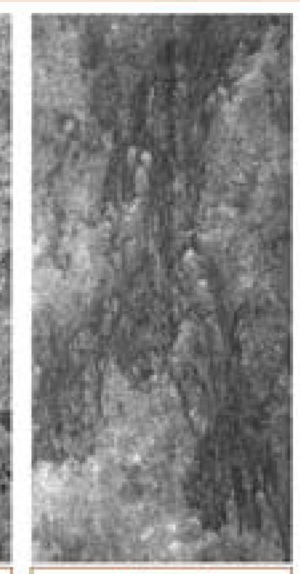

Figure J

Figure K

Figure L: 100 km x 300 km segment of the Belet Dune Field (T8). Parallel orientation and interdune spacing resemble dunes on Earth.

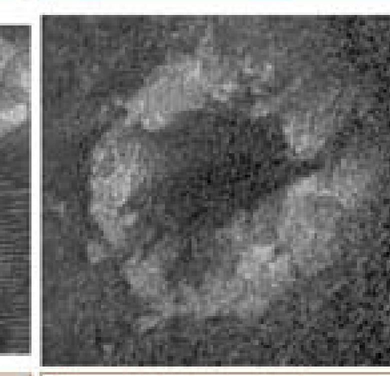

Figure M: Unidentified feature. Catalogued as a discolored ring, but possibly an eroded crater (T13).

Figure I: Lake with porous shoreline and several varying levels of depth. (T16)
Figure J: Dune patches with lower σ_0 than surroundings. Not extended like Belet.(T3)
Figure K: White lines with high reflectivity and dark dune patches between them. (T8)

Features assume many different shapes and sizes; anything that differs from its surroundings could be a feature. Dunes are the most common feature in the regions mapped thus far, but lakes recently debuted in T16. Some features have not been officially identified; for example, the discolored rings *could* be eroded craters but cannot yet be catalogued as such. Collectively, the features exhibit possible cryovolcanism, impact cratering, fluvial processes, aeolian activity, and possible methane cycle activity

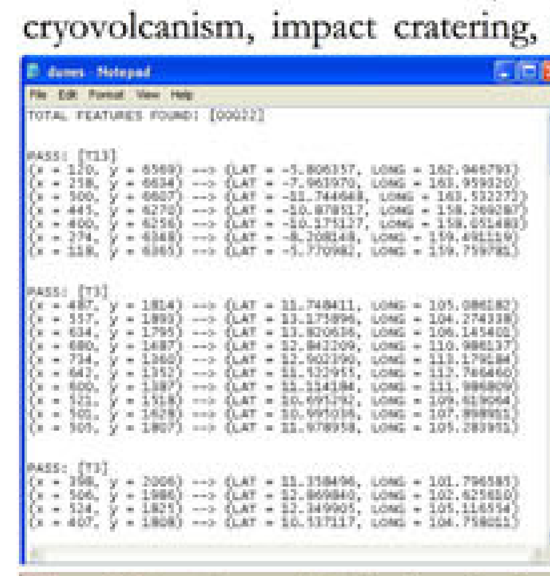

Figure N: First three entries in the 'dunes' catalog.

Features
Circles
Craters
Dunes
Flows
Hills
Lakes
Lines
Marks
Mountains
Peculiarities
Rings

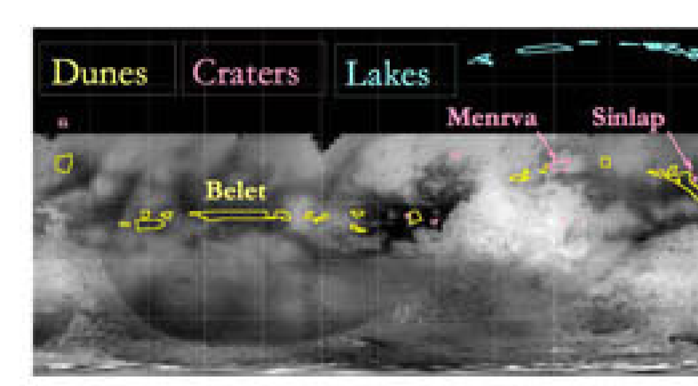

Figure O: Locations of all currently catalogued dune fields, craters, and lakes on Titan's surface. Dunes generally lie in the equatorial region, while lakes seem to favor the poles. We continue to seek trends in the distribution.

Classification of Titan's Surface Regions by Reflectivity

Figure P: Mixed surface on TA, highly suggestive of cryovolcanic flow. Reflectivity (σ_0) varies from ≈0.04 in the darkest to ≈3.02 in the brightest.

Figure Q: Vastly different reflective values exist in adjacent regions (T13). The white area, called Xanadu, is the largest, brightest region on Titan.

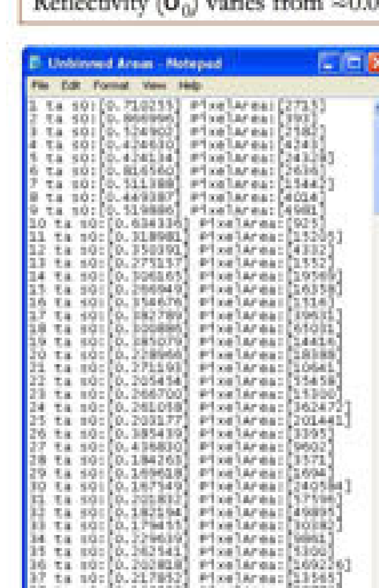

Figure R: Catalog of unbinned TA regions and their average σ_0 values.

Different average σ_0 values separate surface regions of different types. The reflectivity of a surface type is closely related to the surface material and slope. Brighter regions signify higher σ_0 values.

The inpolygon-based averaging algorithm computes average σ_0 for regions given peripheral vertices. We then choose bin ranges so we can group regions of a similar type.

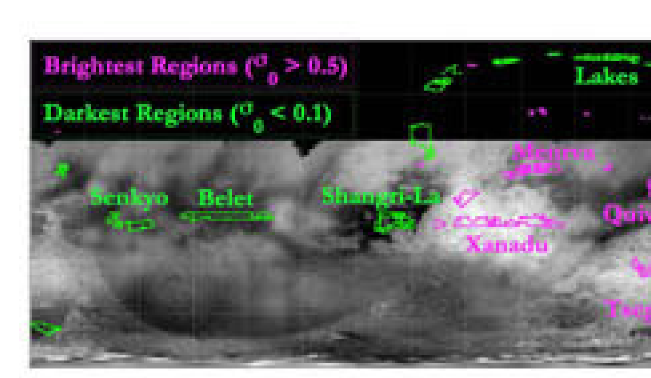

Figure S: Potential application of the surface region σ_0 catalog. After the catalogued areas across all swaths have been divided into bins, we can locate them on a latitude-longitude plot and look for trends in the distribution of regions in a certain σ_0 range. Pictured are the darkest and brightest σ_0 bins observed thus far.

Application of the Catalog to Analysis

We can fit backscatter model curves to the Average σ_0-vs.-Incidence Angle data from the scatterometer to determine the mean dielectric constant and surface slope of several large regions on Titan (Wye, 2006b).

The features catalog and surface reflectivity database could permit more precise analysis; by using σ_0 values from smaller but strongly similar areas, we can determine properties like the dielectric constant and slope for dunes, craters, lakes, bright regions, dark regions, and other groups. We would know exactly where to find them in the scatterometer data since it follows the same latitude-longitude system as the observed SAR data.

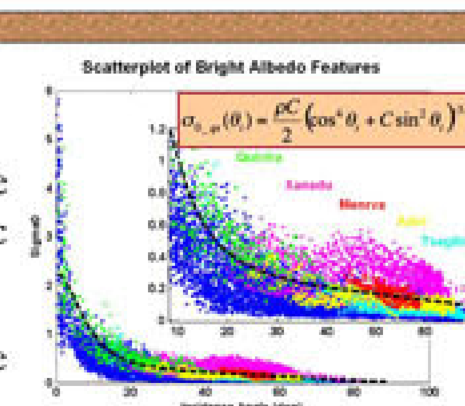

Figure T: Hagfors model curve on scatterometer data for bright regions.

Parameters in the model relate to the mean dielectric constant, RMS surface slope, roughness, etc. (Wye, 2006b).

Please see handout for additional details and references.